International Journal of Pattern Recognition
and Artificial Intelligence
Vol. 26, No. 1 (2012) 1255004 (16 pages)

DOI: 10.1142/S021800141255004X

A LEVEL-SET METHOD BASED ON GLOBAL AND LOCAL REGIONS FOR IMAGE SEGMENTATION

YU QIAN ZHAO*, XIAO FANG WANG*,
FRANK Y. SHIH†,‡ and GANG YU*

*School of Geosciences and Info-Physics
Central South University, Changsha, Hunan 410083, P. R. China

†College of Computing Sciences
New Jersey Institute of Technology, Newark, NJ 07102, USA
‡shih@njit.edu

Received 13 September 2011
Accepted 16 November 2011
Published 18 June 2012

This paper presents a new level-set method based on global and local regions for image segmentation. First, the image fitting term of Chan and Vese (CV) model is adapted to detect the image's local information by convolving a Gaussian kernel function. Then, a global term is proposed to detect large gradient amplitude at the outer region. The new energy function consists of both local and global terms, and is minimized by the gradient descent method. Experimental results on both synthetic and real images show that the proposed method can detect objects in inhomogeneous, low-contrast, and noisy images more accurately than the CV model, the local binary fitting model, and the Lankton and Tannenbaum model.

Keywords: Image segmentation; active contour model; Chan and Vese model; local binary fitting model.

1. Introduction

The active snake model is a variation model in image segmentation. It moves the snake points according to the minimization of sum of internal and external energies integrated along the length of the snake to approach edges. In the original snake formulation of Kass *et al.*,[5] the best snake position was defined as the solution of a variational problem requiring the minimization of sum of internal and external energies integrated along the length of the snake. The corresponding Euler equations, which give the necessary conditions for this minimizer, comprise a force balance equation. The snake model has provided a number of applications in object segmentation, stereo matching, motion tracking, etc. In image processing, the snake model defines a snake as an energy-minimizing spline guided by external constraint forces and influenced by such forces that pull it toward image features such as lines and edges. It is a kind of the active contour model in the way that it locks on nearby edges, localizing them accurately.

One disadvantage of the snake model is "it is incapable of adapting to complex topologies and variable intensity ranged images." Many researchers have proposed alternative methods (for example, See Refs. 17, 18 and 24) to improve the snake model. Caselles *et al.*[2] and Malladi *et al.*[11] developed the *geometric deformable model*, which can be represented implicitly as level-set of Lipchitz functions[13] in the Eulerian fashion. It can handle topological variation and has an efficient numerical scheme to compute energy functions.

The existing active contour models are mainly based on edge information[2,5,11,24] and region intensity information.[3,8,12,15,19–21,23] Region-based active contour models are mostly developed based on Chan and Vese (CV) model,[3] such as Li *et al.*,[8] Pham *et al.*,[15] and Wang *et al.*[21] Therefore, region-based models possess some advantages like anti-noise and independence of the initial active contour position. However, they usually failed to detect object accurately if the objects are subjective to nonuniform illumination and low contrast. To solve this problem, researchers presented various models[6,7,10,22,23,25] by considering local region properties, so-called *local region-based active contour models*. To some extent, they can overcome the intensity inhomogeneity and low contrast. However, most of them are incapable of capturing global minima due to the conversion to local image fitting functions. Paragios and Deriche[14] and Hua *et al.*[4] intended to integrate global properties with the local region-based models, but the computational cost is too high and some complex images present errors. Lin *et al.*[10] applied region probability density with local statistical energy, but their model can only deal with a single object of interest and failed to perform successfully on complex images like medical images.

In this paper, we propose a novel level-set method of integrating both global and local information of an image. The model is set up under the assumption that the objects to be detected must lie inside the current active contour. The image fitting term of CV model is adapted to detect the image's local information by convolving a Gaussian kernel function. A global term is proposed to detect large gradient amplitude at the outer region. The new energy function consists of both local and global terms, and is minimized by the gradient descent method.

The rest of this paper is organized as follows. Section 2 briefly reviews the CV model and the local binary fitting model. Section 3 proposes the improved model. Section 4 presents the experimental results and comparisons. Finally, conclusions are drawn in Sec. 5.

2. Brief Review of CV and LBF Models

The CV model, proposed by Chan and Vese,[3] is based on the Mumford–Shah model.[12] For a given image u_0 on the image domain Ω, CV model's energy functional is represented by two piecewise constant functions:

$$E^{\mathrm{CV}}(C, c_1, c_2) = \lambda_1 \int_{\mathrm{inside}(C)} (u_0(x) - c_1)^2 dx + \lambda_2 \int_{\mathrm{outside}(C)} (u_0(x) - c_2)^2 dx + \mu|C|, \quad (1)$$

where λ_1, λ_2, and μ are positive parameters to balance the terms; $inside(C)$ and $outside(C)$ denote the regions inside and outside the contour, respectively; c_1 and c_2 are the mean intensities inside and outside C, respectively; $|C|$ is the length of curve C.

The CV model uses global region information to detect objects. Its process is independent of the initial position of the active contour. Basically, it is resistant against noise and can segment objects without apparent contour or texture. However, it often misclassifies objects into background when a low-contrast or nonuniform illumination image is occurred. Assume that the parameters in Eq. (1) are $\lambda_1 = \lambda_2 = 1.0$ and $\mu = 0.005 \times 255 \times 255$. An example is shown in Fig. 1(a), where one is a square with intensities darker than background and the other is an ellipse with intensities close to background. From the segmented result in Fig. 1(b), it is observed that CV model can detect the square, whereas miss the ellipse. Another example is shown in Fig. 1(c), where nonuniform illumination is occurred on the same object. From the segmented result in Fig. 1(d), it shows that the object cannot be entirely detected because the CV model only utilizes the global intensity information.

The local binary fitting[7,8] (LBF) model was proposed to enhance the CV model's ability to handle intensity inhomogeneity and low-contrast images. Its main contribution is the use of kernel functions to convert CV model's energy functional, so that it can take advantage of image's local region information to segment inhomogeneous images. Its energy functional is represented as

$$\begin{aligned} E^{\mathrm{LBF}}&(C, f_1(x), f_2(x)) \\ &= \lambda_1 \int \left(\int_{\mathrm{inside}(C)} K(x-y)|u_0(y) - f_1(x)|^2 dy \right) dx \\ &\quad + \lambda_2 \int \left(\int_{\mathrm{outside}(C)} K(x-y)|u_0(y) - f_2(x)|^2 dy \right) dx + \mu|C|, \end{aligned} \quad (2)$$

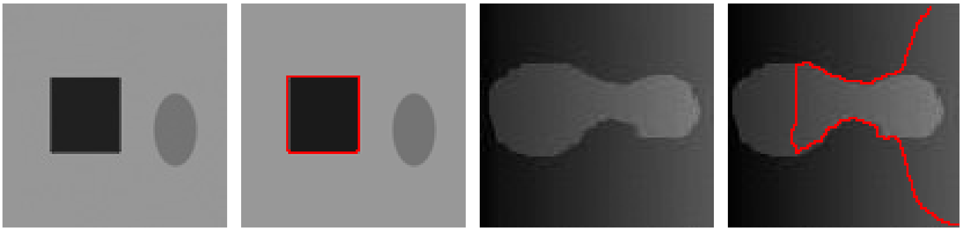

(a) (b) (c) (d)

Fig. 1. Examples of misclassification using CV model. (a) A low-contrast image, (b) segmented result, (c) a nonuniform illumination image, and (d) segmented result.

where λ_1, λ_2, and μ are positive constants; given a center point x, $f_1(x)$ and $f_2(x)$ are the fitting intensities of inner and outer local regions of the detected pixel x, respectively; $u_0(y)$ is the intensity of a local region centered at the point x; $K(x-y)$ is a kernel function which has a larger value when the point y is close to the center point x and decreases to zero when y is far away from x. The following Gaussian kernel function is selected to capture the local information[7]:

$$K_\sigma(z) = \frac{1}{(2\pi)^{n/2}\sigma^n} e^{-|z|^2/2\sigma^2}, \tag{3}$$

where σ is a scale parameter to control the size of local region.

The first two integral terms, namely $\lambda_1 \int(\int_{\text{inside}(C)} K(x-y)|u_0(y) - f_1(x)|^2 dy)dx$ and $\lambda_2 \int(\int_{\text{outside}(C)} K(x-y)|u_0(y) - f_2(x)|^2 dy)dx$ in Eq. (2), denote the LBF energies, and the third term is the curve length used to smooth the active contour. Although LBF can handle the problem caused by intensity inhomogeneity, it cannot solve the problem caused by strong noise or uneven illumination. Since LBF considers the local region information only, the global information is lost.

3. The Proposed Improved Model

3.1. *The global term*

We aim to solve the erroneous detection problem of CV model and LBF model when dealing with low-contrast and nonuniform illumination images. Therefore, a global term, called a penalty function, is proposed to detect the large gradient amplitude at the outer region of the contour. The penalty function is defined as:

$$E^{\text{GL}} = \eta \int_{\text{outside}(C)} |\nabla u_0(x)|^2 dx, \tag{4}$$

where η is a positive parameter used to control the size of the gradient amplitude, and $|\nabla u_0|^2$ is the squared gradient amplitude of the given image. Minimizing Eq. (4) means eliminating the object or part of the object which has large gradient amplitude lying at outside of the active contour. When the contour is convolved by CV model's or LBF model's energy functional, only the mean intensities of inner and outer regions are considered, which may miss some objects with intensity inhomogeneity. However, Eq. (4) can drive the contour to detect the edges or lines, which have large gradient amplitudes at the outer region of the active contour, even if the intensity of the object is close to the background.

To test the performance of the proposed global term, it is natural to combine Eq. (4) with CV model. The new energy function $E^{\mathrm{CV}'}$ can be written as:

$$\begin{aligned} E^{\mathrm{CV}'}(C, c_1, c_2) &= E^{\mathrm{CV}} + E^{\mathrm{GL}} \\ &= \lambda_1 \int_{\mathrm{inside}(C)} | u_0(x) - c_1 |^2 dx + \lambda_2 \int_{\mathrm{inside}(C)} | u_0(x) - c_2 |^2 dx \\ &\quad + \mu|C| + \eta \int_{\mathrm{outside}(C)} |\nabla u_0(x)|^2 dx. \end{aligned} \tag{5}$$

The new energy function is applied to segment the low-contrast image in Fig. 1(a). The initial contour's position shown in Fig. 1(b) is random because CV model's performance is not related to its initialization. CV model's energy is mainly focused on image's intensity, and it does not consider the gradient information such as edges or lines. By adding the term E^{GL}, the improved version of CV model is able to capture the gradient amplitude, which helps to improve the sensitivity to the intensity change. The segmented result in Fig. 2(c) shows that the tendency of misclassification in CV model can be alleviated. Note that there is a small gradient amplitude change around the ellipse's contour, which can be captured by E^{GL}.

3.2. *The proposed level-set framework*

To segment low-contrast images, we use a Gaussian kernel function to convert the CV model's global image fitting term into the local region image fitting function as

$$\begin{aligned} &E^{\mathrm{Local}}(C, f_1(x), f_2(x)) \\ &\quad = \lambda_1 \int \left(\int_{\mathrm{inside}(C)} K_\sigma(x-y) |u_0(y) - f_1(x)|^2 dy \right) dx \\ &\qquad + \lambda_2 \int \left(\int_{\mathrm{outside}(C)} K_\sigma(x-y) |u_0(y) - f_2(x)|^2 dy \right) dx, \end{aligned} \tag{6}$$

where $f_1(x)$ and $f_2(x)$ are the fitting intensities of inner and outer regions near the detected pixel x, respectively, and λ_1 and λ_2 are the positive parameters which

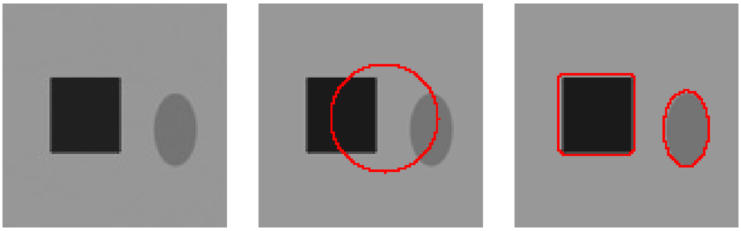

(a) (b) (c)

Fig. 2. The segmented results of the improved CV model. (a) The low-contrast image, (b) initial active contour, and (c) segmented result.

control the influence of intensity difference between the inner and outer regions. Note that $K_\sigma(x-y)$ is defined in Eq. (3).

Thus the proposed framework's energy functional can be represented as

$$\begin{aligned} E &= E^{\mathrm{GL}} + E^{\mathrm{Local}} + \mu|C| \\ &= \eta\int_{\mathrm{outside}(C)} |\nabla u_0(x)|^2 dx + \lambda_1 \int\left(\int_{\mathrm{inside}(C)} K_\sigma(x-y)|u_0(y)-f_1(x)|^2 dy\right)dx \\ &\quad + \lambda_2\int\left(\int_{\mathrm{outside}(C)} K_\sigma(x-y)|u_0(y)-f_2(x)|^2 dy\right)dx + \mu|C|. \end{aligned} \tag{7}$$

For the evolving curve C, we use an implicit representation given by the level-set method,[13] and $C \in \Omega$ is represented implicitly via Lipschitz function $\varphi : \Omega \to R$, such that: $C = \{x \in \Omega | \varphi(x) = 0\}$. Also φ needs to have opposite signs on each side of curve C; for instance, in this paper, φ takes positive and negative values outside and inside of curve C, respectively. Let H be the Heaviside function and use the unknown variable φ to replace the unknown variable C. The energy functional's level-set formulation of Eq. (7) can be expressed as

$$\begin{aligned} E(\varphi, f_1, f_2) = \eta&\int_\Omega |\nabla u_0(x)|^2(1-H(\varphi(x)))dx \\ &+ \lambda_1 \iint K_\sigma(x-y)|u_0(y)-f_1(x)|^2 H(\varphi(y))dx\,dy \\ &+ \lambda_2 \iint K_\sigma(x-y)|u_0(y)-f_2(x)|^2(1-H(\varphi(y)))dx\,dy \\ &+ \mu\int_\Omega |\nabla H(\varphi(x))|dx. \end{aligned} \tag{8}$$

Similarly, Heaviside function H above is approximated by H_ε, which is represented as

$$H_\varepsilon(z) = \frac{1}{2}\left[1 + \frac{2}{\pi}\arctan\left(\frac{z}{\varepsilon}\right)\right], \tag{9}$$

where ε is a positive constant. Note that $\varepsilon = 1.0$ according to the experimental results.

The length of zero level contour $\int_\Omega |\nabla H(\varphi(x))|dx$ can also be represented as $\int \delta_\varepsilon(\varphi(x))|\nabla\varphi(x)|dx$, with the Dirac delta function δ_ε defined by the derivative of H_ε:

$$\delta_\varepsilon(z) = \frac{1}{\pi}\cdot\frac{\varepsilon}{\varepsilon^2 + z^2}. \tag{10}$$

In addition, we utilize the distance regularization term in Li *et al.*[9] to constrain the deviation of the level-set from the signed distance function. The distance can be modeled by

$$P(\varphi) = \int \frac{1}{2}(|\nabla\varphi(x)| - 1)^2 dx. \tag{11}$$

Hence the new energy function is designed to be

$$E^{\text{total}} = E(\varphi, f_1, f_2) + P(\varphi). \tag{12}$$

3.3. *The gradient descent of the proposed model*

By calculating variations, it can be shown that the functions $f_1(x)$ and $f_2(x)$ that minimize the energy functional in Eq. (12) satisfy the following Euler−Lagrange equations:

$$\int K_\sigma(x-y)(u_0(y) - f_1(x))H(\varphi(y))dy = 0 \tag{13}$$

and

$$\int K_\sigma(x-y)(u_0(y) - f_2(x))(1 - H(\varphi(y)))dy = 0. \tag{14}$$

From Eqs. (13) and (14), $f_1(x)$ and $f_2(x)$ are

$$f_1(x) = \frac{\int K_\sigma(x-y)u_0(y)H_\varepsilon(\varphi(y))}{\int K_\sigma(x-y)H_\varepsilon(\varphi(y))dy} \tag{15}$$

and

$$f_2(x) = \frac{\int K_\sigma(x-y)u_0(y)(1 - H_\varepsilon(\varphi(y)))dy}{\int K_\sigma(x-y)(1 - H_\varepsilon(\varphi(y)))dy} \tag{16}$$

which minimize the energy functional in Eq. (12) for a fixed φ.

As $f_1(x)$ and $f_2(x)$ are fixed, minimizing the energy functional E^{total} in Eq. (12) with respect to φ can be achieved by solving the gradient descent flow of Eq. (17). The detailed derivation is available in Appendix A.

$$\begin{aligned}\frac{\partial\varphi}{\partial t} = {} & -\delta_\varepsilon(\varphi)((\lambda_1 e_1 - \lambda_2 e_2) - \eta|\nabla u_0|^2) + \mu\delta_\varepsilon(\varphi)\operatorname{div}\left(\frac{\nabla\varphi}{|\nabla\varphi|}\right) \\ & + \left(\nabla^2\varphi - \operatorname{div}\left(\frac{\nabla\varphi}{|\nabla\varphi|}\right)\right),\end{aligned} \tag{17}$$

where $e_1$and e_2 are the functions:

$$e_1(x) = \int K_\sigma(y-x)|u_0(x) - f_1(y)|^2 dy, \tag{18}$$

$$e_2(x) = \int K_\sigma(y-x)|u_0(x) - f_2(y)|^2 dy. \tag{19}$$

In Eq. (17), the term $-\delta_\varepsilon(\varphi)((\lambda_1 e_1 - \lambda_2 e_2) - \eta|\nabla u_0|^2)$ is derived from local dating fitting energy and global gradient energy, and is responsible to drive the active contour toward object boundaries. The second term $\mu\delta_\varepsilon(\varphi)\mathrm{div}(\nabla\varphi/|\nabla\varphi|)$ is used to maintain the regularity of the contour, and the third term $(\nabla^2\varphi - \mathrm{div}(\nabla\varphi/|\nabla\varphi|))$ is used to maintain the regularity of the level-set function.

All the partial derivatives in Eq. (17) can be simply discretized as central finite difference. The temporal derivative $\partial\varphi/\partial t$ is discretized as a forward difference. The fixed space steps are $\Delta x = \Delta y = 1$, and the time step $\Delta t = 0.1$. In summary, the proposed method's implementation is straightforward, consisting of four steps as:

Step 1. Initialize the parameters λ_1, λ_2, σ, η, μ, and the initial level-set φ_0.
Step 2. Compute $f_1(x)$ and $f_2(x)$ by Eqs. (15) and (16).
Step 3. Solve φ by Eq. (17).
Step 4. Return to Step 2 until the convergence criteria are met.

The convergence criteria are $|\varphi_{n+1} - \varphi_n| \leq T$, where φ_n is zero level-set of the nth iteration, φ_{n+1} is the next iteration of zero level-set, and T is a constant threshold. Note that $T = 0.01$ is used in the experiment.

4. Experimental Results and Comparisons

4.1. *Experiment on synthetic images*

The proposed method is first evaluated on synthetic images as shown in Fig. 3. The following parameters are used: $\lambda_1 = 1.0$, $\lambda_2 = 2.0$, $\eta = 2.0$, $\mu = 0.005$, and $\sigma = 5$. The first column shows different synthetic images with low contrast or ill illumination; the second column shows the initial contour before curve evolution; the third column shows the immediate results. The final segmented results are displayed in the last column. It is observed that the proposed method can detect objects from the images of low-contrast and/or nonuniform illumination.

4.2. *Experiment on real images*

We also test our proposed model on medical images and texture images as shown in Fig. 4. The first row is an ultrasound medical image with the presence of speckle noise and low contrast between objects and background. The second row is a brain image with intensity inhomogeneity. The third row is an image of blood vessel whose contour is weak and blur. The fourth row is a MRI brain image with intensity inhomogeneity. The fifth row is a brain tumor image. The last row is a liver image, which is difficult to segment because the intensities of the adjacent muscle and tissue are close to the liver. From experimental results, it is observed that the proposed model can segment those objects successfully.

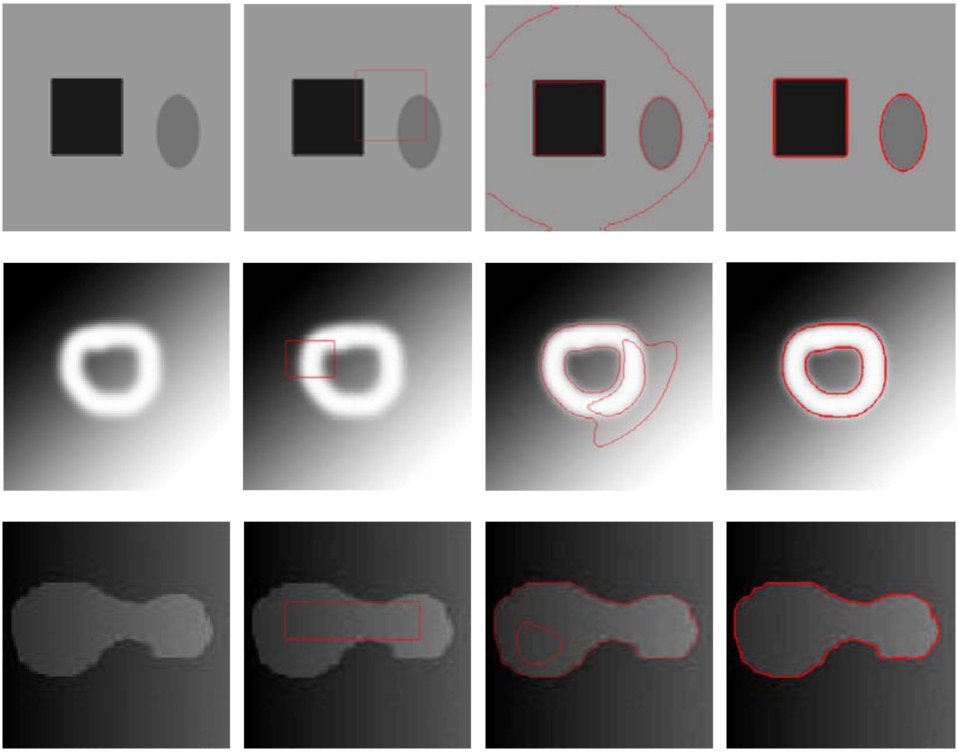

(a) (b) (c) (d)

Fig. 3. Segmentation on different synthetic images. (a) The original images, (b) the initial active contours, (c) the immediate results, and (d) the final results.

In addition, we perform evaluation on texture images as shown in Fig. 5. The first row is a panther puma image whose pattern is similar to the background. The second row is a tiger image subjective to nonuniform illumination, in which the tiger's stripe pattern is similar to the water wave.

4.3. *Comparison with level-set methods*

The proposed method is compared with two famous level-set methods: CV model and LBF model, as shown in Figs. 6 and 7, respectively. The initial contour of CV model is a circle with center $[ic, jc]$ and radius $r = ic/3$, where $ic = n\,Row/2$, $jc = n\,Col/2$ and the size of the image is $nRow \times nCol$. The LBF model's initial contours are the same as the second column of Figs. 4 and 5. From Fig. 6, it can be seen that CV model fails to segment most of the images using only global information. Based on local information, LBF model performs better than CV model; however, it fails to segment liver (the sixth image) and tiger (the last image) as shown in Fig. 7. Obviously, the proposed method can extract object successfully from those images in Figs. 4 and 5.

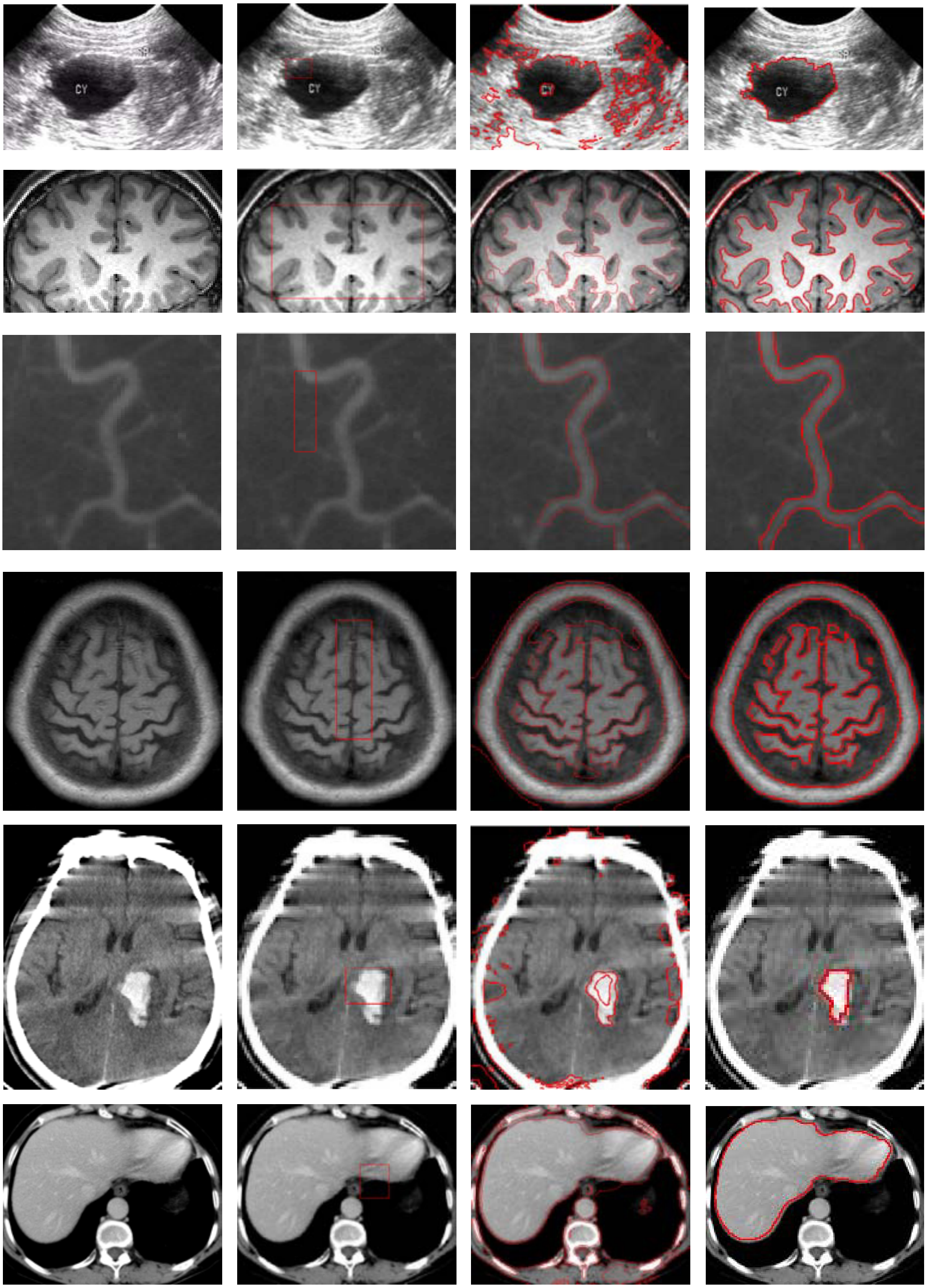

(a) (b) (c) (d)

Fig. 4. Segmentation on different medical images. (a) The original images, (b) the initial active contours, (c) the immediate results, and (d) the final results.

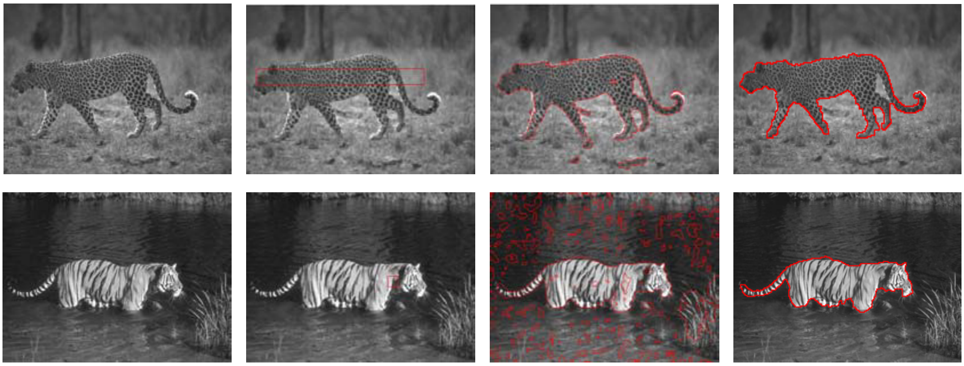

(a) (b) (c) (d)

Fig. 5. Segmentation on different texture images. (a) The original images, (b) the initial active contours, (c) the immediate results, and (d) the final results.

4.4. *Comparisons on noisy synthetic images*

We also conduct comparisons of our proposed method against CV model,[3] LBF model,[10] and Lankton and Tannenbaum[6] model using the synthetic images delineated by Gaussian noise, as shown in Fig. 8. The four models are compared using Gaussian noise with standard deviations: 0.022, 0.037, 0.043, and 0.056, respectively. Columns (b)–(e) show the segmented results by Chan and Vese,[3] Li *et al.*,[8] Lankton and Tannenbaum,[6] and our proposed model, respectively. It is observed that Chan and Vese[3] and Lankton and Tannenbaum[6] are unable to segment the ellipse from the different noise-delineated images, and Li *et al.*[8] can segment the ellipse in the first three noisy images. The proposed model can segment both objects from all noisy images successfully.

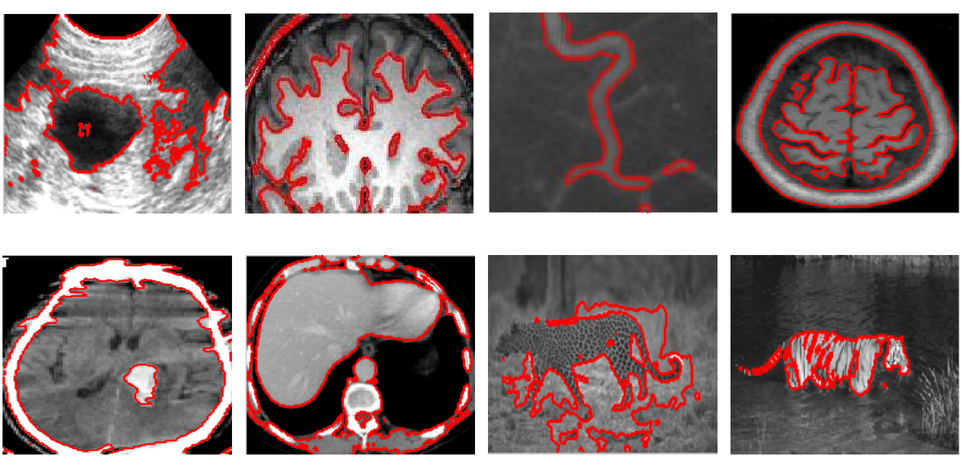

Fig. 6. Segmentation on different images with CV model.

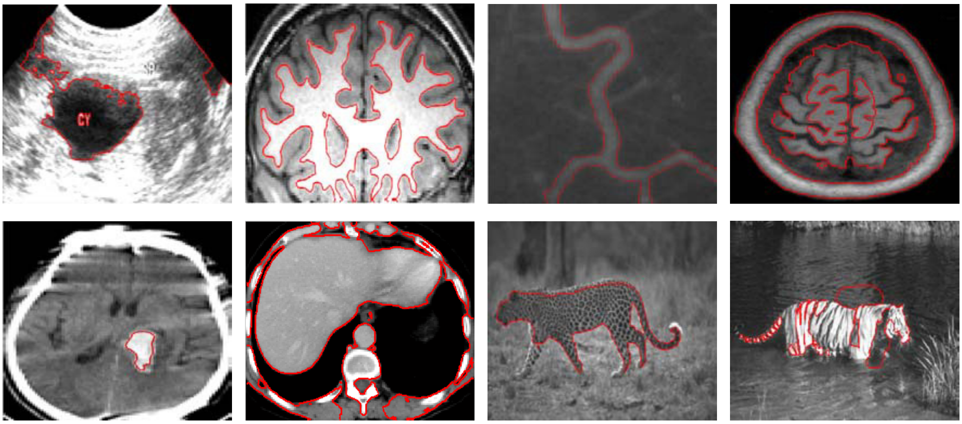

Fig. 7. Segmentation on different images with LBF model.

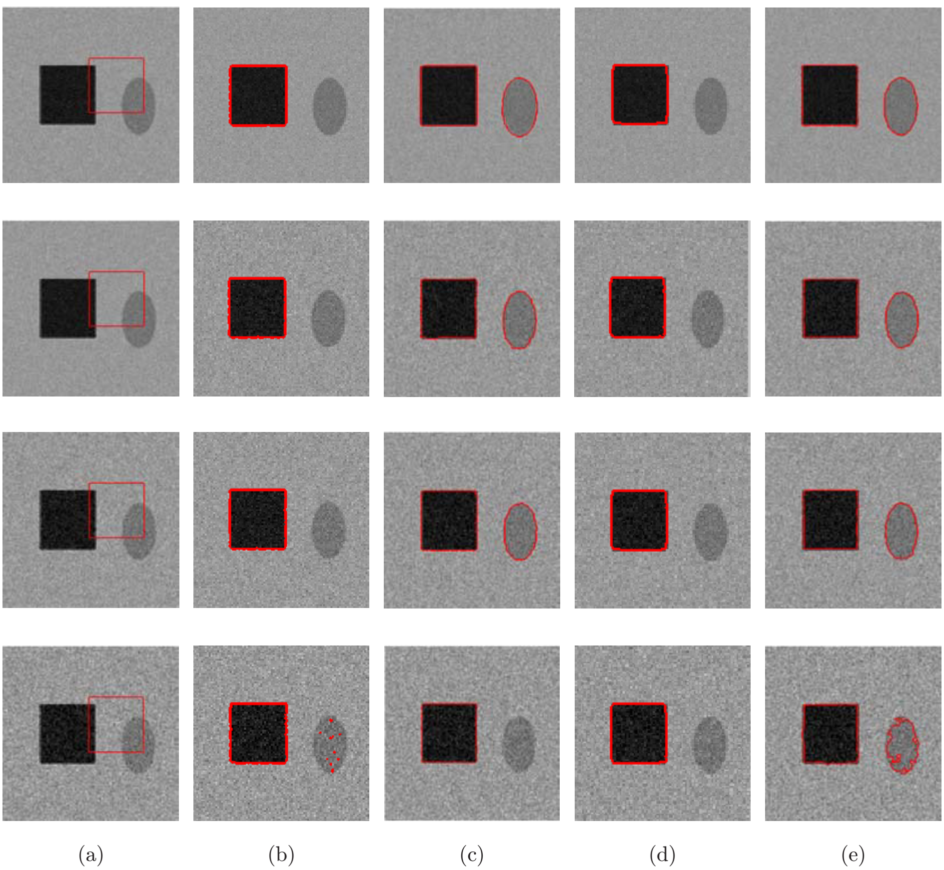

Fig. 8. Comparisons on Gaussian noisy images. (a) The initial active contours, (b) the results by CV model,[3] (c) the results by LBF model,[10] (d) the results by Lankton and Tannenbaum model,[6] and (e) the results by our proposed model. See context for details.

Table 1. The AERs of CV model, LBF model, Lankton and Tannenbaum model,[6] and the proposed model.

	std = 0.022		std = 0.037		std = 0.043		std = 0.056	
Model	Square	Ellipse	Square	Ellipse	Square	Ellipse	Square	Ellipse
CV model	0.0968	1.0000	0.0934	1.0000	0.0922	1.0000	0.0886	1.0000
LBF model	0.1557	0.1592	0.1400	0.1531	0.1340	0.1509	0.1329	0.0673
L-T (2008)	0.1941	1.0000	0.1879	1.0000	0.1968	1.0000	0.2051	1.0000
The proposed model	0.0646	0.1176	0.0645	0.1109	0.0646	0.1143	0.0673	0.2748

For further comparisons, the *area error rate* (AER)[16] is used as a measure metrics:

$$\mathrm{AER} = \frac{\mathrm{RU} - \mathrm{RI}}{\mathrm{RT}}, \tag{20}$$

where $\mathrm{RU} = \mathrm{RA} \cup \mathrm{RT}$, $\mathrm{RI} = \mathrm{RA} \cap \mathrm{RT}$, RA denotes the region segmented from an algorithm, and RT denotes the ground-truth region. The smaller the AER, the better the detection of an algorithm.

The mean AER value is computed using 10 images delineated by the same Gaussian standard deviation. The parameters for CV model are: $\lambda_1 = 1.0$, $\lambda_2 = 1.0$, $\mu = 0.005 \times 255 \times 255$, and for LBF model are: $\lambda_1 = 1.0$, $\lambda_2 = 2.0$, $\mu = 0.01 \times 255 \times 255$, $\sigma = 5$. The local radius for Lankton and Tannenbaum model[6] is 13 pixels. The parameters for our proposed model are: $\lambda_1 = 1.0$, $\lambda_2 = 2.0$, $\sigma = 5$, $\eta = 2.0$, $\mu = 0.001$. The overall AER results are listed in Table 1, from which it can be noted that the mean AER of our proposed model is the smallest, indicating the best detection accuracy. Note that the mean AER of CV model and Lankton and Tannenbaum model[6] on the detected ellipse is 1, indicating failure to segment the ellipse.

5. Conclusion

In this paper, we propose a region-based level-set method which considers both global and local information of an image. We utilize the Gaussian kernel function to detect the intensity difference on the image's local region based on the CV model's global term. We also introduce a new penalty function which eliminates the large amplitude gradient on the outer region of the active contour. The experiments conducted on synthetic and real images show that the proposed method can segment objects in intensity inhomogeneous and low-contrast images successfully. Furthermore, the performance of the proposed model is superior to CV model, LBF model, and Lankton and Tannenbaum model[6] when dealing with strong noise background.

Acknowledgments

This work is supported by the National Natural Science Foundation of China (Grant No. 61172184), China Postdoctoral Science Foundation Specially Funded Project

(200902482), Hunan Provincial Natural Science Foundation of China (09JJ3119), and Central South University fund for freedom of exploration program (201011200144).

Appendix A. Derivation of Gradient Flow

In order to minimize the energy functional $F(\varphi)$, we solve the gradient flow equation as

$$\frac{\partial \varphi}{\partial t} = -\frac{\partial F}{\partial \varphi}, \tag{A.1}$$

where $\partial F/\partial\varphi$ is the Grâteaux derivative[1] of the energy functional $F(\varphi)$. We need to derive the Grâteaux derivative of the global term $\eta\int_\Omega |\nabla u_0(x)|^2(1-H(\varphi(x)))dx$ in Eq. (8). By calculating variations,[1] it is straightforward to derive the Grâteaux derivative of the energy E^{GL} as

$$\frac{\partial E^{\mathrm{GL}}}{\partial \varphi} = \eta\delta_\varepsilon(\varphi)|\nabla u_0(x)|^2. \tag{A.2}$$

A combination of the Grâteaux derivatives of the three terms in the entire energy functional yields

$$\begin{aligned}\frac{\partial E^{\mathrm{total}}}{\partial \varphi} &= \delta_\varepsilon(\varphi)[(\lambda_1 e_1 - \lambda_2 e_2) - \eta|\nabla u_0|^2] \\ &\quad - \mu\delta_\varepsilon(\varphi)\mathrm{div}\left(\frac{\nabla\varphi}{|\nabla\varphi|}\right) - \left(\nabla^2\varphi - \mathrm{div}\left(\frac{\nabla\varphi}{|\nabla\varphi|}\right)\right).\end{aligned} \tag{A.3}$$

Using Eq. (A.1) for the energy functional E^{total}, its gradient flow of Eq. (17) can be obtained.

References

1. G. Aubert and P. Kornprobst, *Mathematical Problems in Image Processing: Partial Differential Equations and the Calculus of Variations*, 2nd edn., Applied Mathematical Sciences, Vol. 147 (Springer, New York, 2006).
2. V. Caselles, R. Kimmel and G. Sapiro, Geodesic active contours, *Int. J. Comput. Vis.* **22**(1) (1997) 61–79.
3. T. F. Chan and L. A. Vese, Active contours without edges, *IEEE Trans. Image Process.* **10**(2) (2001) 266–277.
4. G. Hua, Z. Liu, Z. Zhang and Y. Wu, Iterative local-global energy minimization for automatic extraction of objects of interest, *IEEE Trans. Patt. Anal. Mach. Intell.* **28**(10) (2006) 1701–1706.
5. M. Kass, A. Witkin and D. Terzopoulos, Snakes: Active contour models, *Int. J. Comput. Vis.* **1**(4) (1988) 321–331.
6. S. Lankton and A. Tannenbaum, Localizing region-based active contours, *IEEE Trans. Image Process.* **13**(11) (2008) 2029–2039.
7. C. M. Li, C. Y. Kao, J. C. Gore and Z. H. Ding, Implicit active contours driven by local binary fitting energy, *IEEE Conf. Computer Vision and Pattern Recognition* (2007), pp. 1–7.

8. C. Li, C. Y. Kao, J. C. Gore and Z. H. Ding, Minimization of region-scalable fitting energy for image segmentation, *IEEE Trans. Image Process.* **17**(10) (2008) 1940–1949.
9. C. M. Li, C. Y. Xu, C. F. Gui and M. D. Fox, Level-set evolution without re-initialization: A new variational formulation, *IEEE Computer Society Conf. Computer Vision and Pattern Recognition* (2005), pp. 430–436.
10. Y. Lin, Y. Yang and X. Wang, A fast active contour model driven by global-local statistical energy, *Second Int. Symp. Intelligent Information Technology Application* (2008), pp. 407–411.
11. R. Malladi, J. A. Sethian and B. C. Vemuri, Shape modeling with front propagation: A level-set approach, *IEEE Trans. Patt. Anal. Mach. Intell.* **17**(2) (1995) 158–175.
12. D. Mumford and J. Shah, Optimal approximations by piecewise smooth functions and associated variational problems, *Commun. Pure Appl. Math.* **42**(5) (1989) 577–685.
13. S. Osher and J. A. Sethian, Fronts propagating with curvature-dependent speed: Algorithms based on Hamilton–Jacobi formulations, *J. Comput. Phys.* **79**(1) (1988) 12–49.
14. N. Paragios and R. Deriche, Geodesic active regions: A new framework to deal with frame partition problems in computer vision, *J. Vis. Commun. Image Represent.* **13**(1–2) (2002) 249–268.
15. V. T. Pham, T. T. Tran, Y. J. Chiu and K. K. Shyu, Region-aided geodesic active contour model for image segmentation, *IEEE Int. Conf. Computer Science and Information Technology* (2010), pp. 318–321.
16. K. Seo, L. Ludeman, C. S. Park and J. Park, Efficient liver segmentation based on the spine, Lecture Notes in Computer Science, Vol. 3261 (2005), pp. 400–409.
17. F. Y. Shih and K. Zhang, Efficient contour detection based on improved snake model, *Patt. Recogn. Artif. Intell.* **18**(2) (2004) 197–209.
18. F. Y. Shih and K. Zhang, Locating object contours in complex background using improved snakes, *Comput. Vis. Image Understand.* **105**(2) (2007) 93–98.
19. Y. Tian, M. Q. Zhou, Z. K. Wu and X. C. Wang, A region-based active contour model for image segmentation, *Int. Conf. Computational Intelligence and Security* (2009), pp. 376–380.
20. L. A. Vese and T. F. Chan, A multiphase level-set framework for image segmentation using the Mumford and Shah model, *Int. J. Comput. Vis.* **50**(3) (2002) 271–293.
21. L. Wang, L. He, A. Mishra and C. Li, Active contours driven by local Gaussian distribution fitting energy, *Signal Process.* **89**(12) (2009) 2435–2447.
22. X. F. Wang, D. S. Huang and H. Xu, An efficient local Chan–Vese model for image segmentation, *Patt. Recogn.* **43**(3) (2010) 603–618.
23. H. Wang, M. Liu and S. Zhu, Medical image segmentation using active contour driven by local energy and minimal variance, *Int. Asia Conf. Informatics in Control, Automation and Robotics* (2010), pp. 40–43.
24. C. Xu and J. L. Prince, Snakes, shapes, and gradient vector flow, *IEEE Trans. Image Process.* **7**(3) (1998) 359–369.
25. K. Zhang, H. Song and L. Zhang, Active contours driven by local image fitting energy, *Patt. Recogn.* **43**(4) (2010) 1199–1206.

Yu Qian Zhao received the Ph.D. degree from Central South University, Changsha, China, in 2006. He engaged in postdoctoral research at Xiangya School of Medicine, Changsha, China, from May 2007 to June 2009, and at New Jersey Institute of Technology, Newark, New Jersey, USA, from July 2009 to July 2010. He is currently an Associate Professor in the College of Geosciences and Info-Physics, Central South University.

His research interests include image processing, pattern recognition, computer vision, image forensics, and computer-aided diagnosis.

Xiao Fang Wang received B.S. from Central South University, Changsha, China, in June 2009, and M.S. from Central South University, Changsha, China, in June 2011. She is presently a Ph.D. student at Ecole Central de Lyon, Lyon, France.

Her current research interests include image processing, graph partitioning, and pattern recognition.

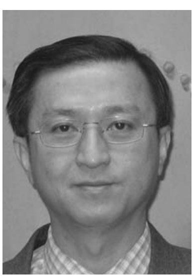

Frank Y. Shih received B.S. from National Cheng Kung University, Tainan, Taiwan, in 1980, M.S. from State University of New York, Stony Brook, USA, in 1983, and Ph.D. from Purdue University, West Lafayette, IN, USA, in 1987. He is presently a professor jointly appointed in the Department of Computer Science, the Department of Electrical and Computer Engineering, and the Department of Biomedical Engineering at New Jersey Institute of Technology, Newark, New Jersey. He is also Director of Computer Vision Laboratory. Dr. Shih held a visiting professor position at Princeton University, Columbia University, National Taiwan University, National Institute of Informatics, Tokyo, Conservatoire National Des Arts Et Metiers, Paris, and Central South University, Changsha, China. He is an internationally renowned scholar and serves as the Editor-in-Chief for the *International Journal of Multimedia Intelligence and Security* (*IJMIS*). Dr. Shih is currently on the editorial board of *Pattern Recognition, Pattern Recognition Letters, the International Journal of Pattern Recognition and Artificial Intelligence, Journal of Information Hiding and Multimedia Signal Processing, Recent Patents on Engineering, Recent Patents on Computer Science, The Open Nanoscience Journal, the International Journal of Internet Protocol Technology, the Journal of Internet Technology, ISRN Signal Processing, and ISRN Machine Vision.* He served as a steering member, committee member, and session chair for numerous professional conferences and workshops. He has received numerous grants from the National Science Foundation, Navy and Air Force, and Industry. He is the recipient of Research Initiation Award of NSF in 1991 and Board of Overseers Excellence in Research Award of NJIT in 2009.

Dr. Shih has made significant contributions to information hiding, focusing on the security and robustness of digital watermarking and steganography. He authored three books: *Digital Watermarking and Steganography*, *Image Processing and Mathematical Morphology*, and *Image Processing and Pattern Recognition*, and edited a book: *Multimedia Security: Watermarking, Steganography, and Forensics*. He published 115 journal papers, 95 conference papers, and 10 book chapters.

His current research interests include image processing, computer vision, watermarking and steganography, digital forensics, sensor networks, pattern recognition, bioinformatics, information security, robotics, fuzzy logic, and neural networks.

Gang Yu received the Ph.D. degree from Xi'an Jiaotong University, Xi'an, China in 2006. He engaged in postdoctoral research at Xi'an Jiaotong University, Xi'an, China, from October 2008 to November 2011. He is currently an Associate Professor in the College of Geosciences and Info-Physics, Central South University. His research interests include medical imaging and image process, computer vision.